Structural and quantitative analysis of stainless steel coatings deposited by DC-magnetron sputtering in a reactive atmosphere

Terwagne, Guy; Hody, Hubert; Colaux, Julie

Published in:
Surface and Coatings Technology

Publication date:
2003

Document Version
Peer reviewed version

Available online at www.sciencedirect.com
SCIENCE DIRECT®
Surface and Coatings Technology 174–175 (2003) 383–388
SURFACE & COATINGS TECHNOLOGY
www.elsevier.com/locate/surfcoat

Structural and quantitative analysis of stainless steel coatings deposited by DC-magnetron sputtering in a reactive atmosphere

G. Terwagne*, H. Hody, J. Colaux

Laboratoire d'Analyses par Réactions Nucléaires, Facultés Universitaires Notre-Dame de la Paix, 61, rue de Bruxelles-B-5000 Namur, Belgium

Abstract

Stainless steel coatings were deposited on low carbon steel and thin SiO_2 substrates by DC-magnetron sputtering in a reactive atmosphere containing argon, nitrogen and hydrogen. The total mass flow of nitrogen was kept constant (8 sccm) for all depositions and the hydrogen mass flow was varied between 0 and 9 sccm while argon mass flow was chosen to obtain a total pressure of 0.28 Pa in the chamber. The elemental composition of coatings and the deposition rates were studied by Rutherford backscattering (RBS), by X-ray emission induced by charge particles (PIXE), by nuclear reactions (NRA) and by resonant nuclear reactions (RNRA). The hydrogen and nitrogen contents in the deposited layers are found to increase with increasing hydrogen mass flow and the deposition rates are decreased with decreasing of argon mass flow. The hydrogen depth profiles in the coatings show an accumulation of hydrogen located at the surface and the interface. A structural analysis by means of conversion electron Mössbauer spectroscopy (CEMS) was also performed. The results indicate that some minor structural modifications were observed when the mass flow of hydrogen was increased.

Keywords: PVD; Magnetron sputtering; Stainless steel; Nitrogen; Hydrogen

1. Introduction

Austenitic stainless steels are well known for their corrosion resistant qualities but their poor wear resistance limits their performance. Nitriding of these steels can be performed by several techniques such as conventional ion implantation [1–4], pulsed plasma nitriding [5] and plasma immersion ion implantation (PI^3) [6]. As long as the treatment temperature is kept below a critical value of approximately 450 °C, the wear resistance can be improved without compromising the corrosion performance. At these lower temperatures, nitrogen remains in solid solution, producing a phase that has been variously called 'S-phase' [7], 'expanded austenite' [8], or γ_N phase [3,4].

Magnetron sputtering offers new possibilities and more flexibility for producing coatings on various substrates at low temperature. While coatings sputtered from austenitic stainless steel targets at low temperature usually form a ferritic bcc structure [9], addition of nitrogen to the sputtering gas results in a nitrogen supersaturated fcc phase with improved wear resistance and higher corrosion resistance [10–12]. These coatings, whose properties and structure are similar to the 'S-phase' produced by nitriding, can be produced by DC-magnetron sputtering using stainless steel targets.

The purpose of this paper is to study the influence of hydrogen on the growth of nitrided stainless steel coatings and to produce a more effective nitrogen phase. In a previous work, we have shown that the deposition rate of the nitrided stainless steel depends on nitrogen mass flow [13]. Typical deposition rate approximately 2.4×10^{15} at. cm^{-2} s^{-1} were observed for a DC-magnetron power of 100 W and nitrogen mass flow lower than 25% of the total sputter and reactive gases in the chamber. We can double the deposition rate if we double the DC-magnetron power, but it is also possible to increase the deposition rate when hydrogen is added to the reactive gas [14]. This investigation shows that some improvement in nitriding efficiency can be obtained when less than 10% of hydrogen is added to the reactive and sputter gases. Elemental composition analysis is realised by nuclear reaction analysis (NRA), resonant nuclear reaction analysis (RNRA), X-ray emission induced by charge particles (PIXE) and Rutherford

*Corresponding author. Tel.: +32-81-72-5478; fax: +32-81-72-5474.
E-mail address: guy.terwagne@fundp.ac.be (G. Terwagne).

0257-8972/03/$ - see front matter © 2003 Elsevier Science B.V. All rights reserved.
doi:10.1016/S0257-8972(03)00594-2

backscattering spectroscopy (RBS), whereas structural analysis is performed by means of conversion electron Mössbauer spectroscopy (CEMS).

2. Sample preparation

The coatings were deposited using an unbalanced DC-magnetron sputtering system placed in a small chamber of 0.05 m^3 equipped with a 280 l/s turbo-molecular pump which provides a base pressure of 10^{-5} Pa. A 50 mm diameter AISI-304L (composition in wt.%-Fe:70%, Cr:18%, Ni:10% and Mn:2%) disk target was placed just above the magnets with a good thermal contact to the holder in order to cool the magnetic material with water during deposition. The source to sample holder distance was 150 mm and a chimney was placed on the top of the target to prevent contamination of the whole chamber. A shutter was placed between the top of chimney and the sample holder in order to avoid deposition during target cleaning for 5 min before each deposition.

Two sets of substrates were used in this study:

a. SiO_2 disk (20 mm in diameter) of 200 μm thick to measure the deposition rates and the elemental analysis of the coatings,
b. Low carbon steel for the elemental and structural analysis.

The low carbon steel disk of diameter 20 mm and thickness 0.25 mm were mechanically polished with diamond paste (15 and 1 μm) and then with alumina powder (0.5 μm). The substrates were cleaned in an ultrasonic bath with pentane before loading into the chamber. Prior to each deposition, the substrates were etched for 2 min in order to remove oxide from the steel surface and to enhance coating adhesion.

Depositions were made at room temperature in the same conditions for both sets of substrates. The magnetron power was set to 200 W during deposition and the voltage applied to the sputter target was approximately −500 V. Although the substrate was heated by electron and ion bombardment, the temperature was measured below 100 °C during deposition with a thermocouple placed at the rear of the specimen. The coatings were reactively deposited during 15 min with various $Ar/N_2/H_2$ gas mixtures, which give various thicknesses, which can be related to the Ar flow (see below). The N_2 flow in the sputter gas was kept constant at 8 sccm for all specimens, while the proportion of H_2 was varied by changing the H_2 flow rate, with compensating adjustment of the Ar flow rate, such that the total pressure remains constant in the chamber (Table 1). These flows correspond to a total pressure of 0.28 Pa measured with a baratron gauge placed in the deposition chamber. The partial pressure of Ar, N_2, H_2 and other residual gases were measured using a 7 mtorr Micropole Analyser with 1.2 amu resolution. Fig. 1 shows the partial pressure of Ar, N_2 and H_2 vs. H_2 flow. It is clearly observed that the Ar partial pressure is drastically

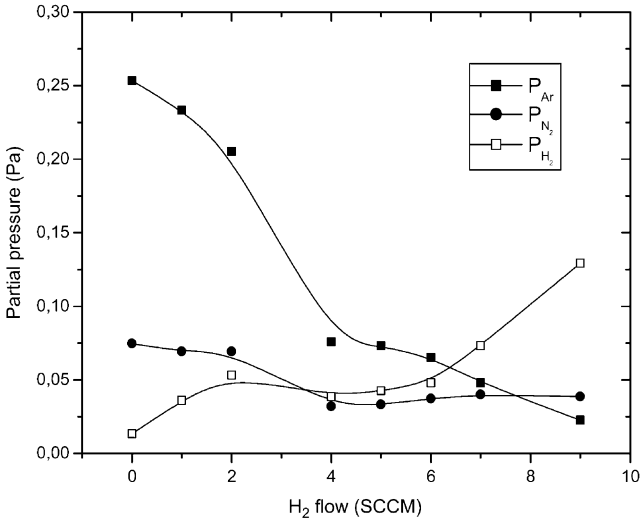

Fig. 1. Partial pressures of Ar, N_2 and H_2 as a function of hydrogen mass flow.

Table 1
Relative amount of Fe, Cr, Ni, N and H measured for different coatings

Coating number	Ar flow (sccm)	N_2 flow (sccm)	H_2 flow (sccm)	[Fe] (at.%)	[Cr] (at.%)	[Ni] (at.%)	[N] (at.%)	[H] (at.%)
1	28.0	8	0	46.5	10.0	4.5	28	8
2	28.0	8	1	46.5	10.0	4.5	28	8
3	26.0	8	2	47.5	10.0	4.5	30	5
4	18.8	8	3	48.0	10.5	4.5	30	7
5	17.1	8	4	46.5	9.5	4.0	31	7
6	16.2	8	5	46.5	9.5	4.0	31	7
7	12.5	8	6	46.5	9.5	4.0	31	7
8	9.7	8	7	46.5	9.5	4.0	32	8
9	4.2	8	9	42.5	7.5	3.0	32	15

Nitrogen flow is kept constant while hydrogen flow is increased. The argon flows have been set to keep constant the total pressure in the chamber.

decreasing when the H_2 flow is increasing. This effect will certainly affect the deposition rates (Section 3).

3. Coatings characterisation

3.1. Elemental analysis

Nuclear elemental analyses were performed at LARN with the 2 MV Tandetron ALTAÏS accelerator ('Accélérateur Linéaire Tandetron pour l'Analyse et l-'Implantation des Solides'). The thickness and composition of the coatings were measured by RBS and PIXE techniques with 2 MeV incident α particles. These measurements were made on the coatings deposited on SiO_2 substrates to avoid interfering signals from the substrate. The scattered particles were detected in a passivated implanted planar silicon detector (PIPS) at 175° relative to the incident beam. By fitting the experimental spectrum, it was possible to obtain the thickness of the coating. The deposition rates were then calculated and are presented in Fig. 2a. The deposition rate of nitrided stainless steel is linearly decreasing when the H_2 flow is increased. As it was suggested above, this effect is mainly due to the decreasing of Ar flow in order to keep the total pressure constant. The relative amount of Cr, Fe and Ni, reported in Table 1, were measured by PIXE technique, simultaneously during RBS measurements, with a X-flash Si(Li) detector placed at 135° relative to incident beam. In Fig. 2b, we can observe that the relative concentrations of Fe, Cr and Ni are slowly decreased. The relative proportion of Fe, Cr and Ni are identical to the target cathode.

Nuclear reaction analysis (NRA) was used to measure the nitrogen concentration using $^{14}N(\alpha,p)^{17}O$ at 4.8 MeV. Although endoenergetic ($Q=-1.191$ MeV), this nuclear reaction is suitable for nitrogen analysis because it shows a constant cross-section (5 mb/sr) at 90° for incident energies ranging between 4.6 and 4.8 MeV [15]. The protons were detected in a PIPS detector placed at 90° relatively to the incident beam. A 24.4 μm mylar absorber was placed in front of the particle detector to avoid elastic scattered particles in the PIPS detector. The nitrogen concentrations are also reported in Table 1.

To depth profile nitrogen, we have used the $^{15}N(p,\alpha\gamma)^{12}C$ resonant nuclear reaction at proton energy of 429 keV. This reaction is revealed by the specific 4.43 MeV γ-rays of the ^{12}C. To obtain an excitation curve at high resolution, the incident particle energy is increased by small increments starting from near-resonance energy. Voltage steps of 500 V are then applied to the terminal of the tandem accelerator. A liquid nitrogen trap is mounted in front of the sample in order to reduce carbon contamination and γ-rays are detected in 4×4 inch NaI detector [16]. The excitation curves obtained depend on the natural width of the resonance

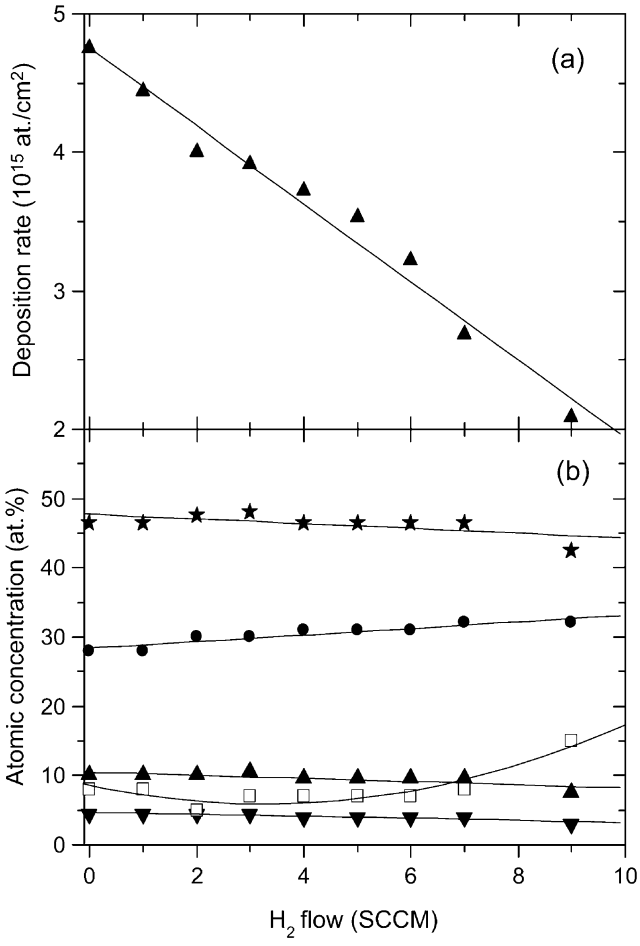

Fig. 2. (a) Deposition rates measured by RBS as a function of hydrogen flow; (b) atomic concentration of Fe (★), Cr (▲) and Ni (▼) measured by PIXE, N (●) measured by NRA and H (□) measured by RNRA vs. the hydrogen mass flow. The solid lines have been drawn as a guide for the eyes.

(Γ_R), on the Doppler broadening (Γ_D), on the energy spread of the beam (Γ_B) and on the straggling effect (Γ_S) due to unequal energy loss of identical particles. In our case, the natural width ($\Gamma_R=120$ eV) and the Doppler broadening ($\Gamma_D=90$ eV) at room temperature are both well known or easily estimated with the classical expression [17]. The beam energy spread is approximately $\Gamma_B=60$ eV on the basis of the accelerator specifications. If any upper contamination layer has been formed, the last parameter Γ_S corresponds exclusively to the energy lost in the nitride deposited on the substrate surface. To obtain the physical distribution from the excitation curves, we have to extract the straggling part from the total excitation peak width; it has been assumed that all these contributions are Gaussian-like [18]. Furthermore, the height of the excitation yield can then be immediately correlated with the ^{15}N concentration in the atom layers probed by the proton beam. Typical physical nitrogen depth profiles are pre-

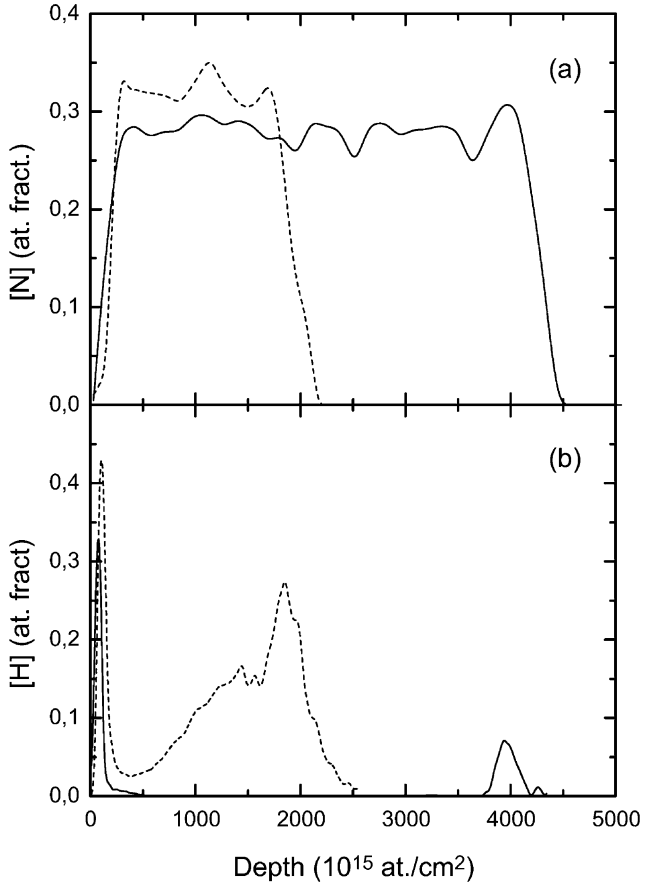

Fig. 3. (a) Depth profiling of nitrogen measured with $^{15}N(p,\alpha\gamma)^{12}C$ resonant nuclear reaction for the coatings deposited without hydrogen mass flow (solid line—first coating in Table 1) and with 9 sccm hydrogen flow (dashed line—last coating in Table 1), (b) Depth profiling of hydrogen measured with the reverse $^{1}H(^{15}N,\alpha\gamma)^{12}C$ resonant nuclear reaction for the same coatings as in (a).

sented in Fig. 3a (samples 1 and 9). For all coatings, the nitrogen depth distributions are still constant in the nitrided layer but the thickness and the nitrogen concentration in the coatings are correlated to the hydrogen flows. The thickness of the nitrided layers, 2000 and 4500×10^{15} at. cm^{-2}, respectively, can be directly correlated with the deposition rates shown in Fig. 2a. The ratio between the deposition rates of coatings 1 and 9 is the same as the ratio between the thickness of both layers and the deposition time was the same for all coatings.

The hydrogen depth profiling was performed with the reverse resonant reaction mentioned above, $^{1}H(^{15}N,\alpha\gamma)^{12}C$. The resonant energy is 6.385 MeV and the depth profile was obtained in the same geometry than for nitrogen depth profiling. The $^{15}N^{3+}$ or $^{15}N^{4+}$ beam was produced by ALTAÏS after cutting and stripping the $C^{15}N^{-}$ ion in the stripper canal of the tandem. $C^{15}N^{-}$ anion is a very prolific ion produced by the Cs sputter source when a mixture of $Ti^{15}N$ and C powder is used as sputter material. Typical beam current of 100 and 10 nA can be obtained for $^{15}N^{3+}$ and $^{15}N^{4+}$ ions, respectively. A maximum energy of 9.130 MeV for $^{15}N^{4+}$ ion provides a depth profile on more than 1 μm range. Physical depth profiles of hydrogen presented in Fig. 3b have also been corrected to take into account for desorption of hydrogen during heavy ion irradiation. It has been shown that hydrogen concentration decreases exponentially at the surface of the layer and linearly at the interface. As we are interested in the hydrogen concentration in the coating, we have only used the linear correction for depth profiling hydrogen.

3.2. Structural analysis

CEMS was used to determine the different phases formed after deposition of the nitrogen-rich stainless steel coatings on the low carbon steel substrates. As it is well known, CEMS is most sensitive to the top 0.1 μm (nearly 80% of conversion electrons are produced in this top layer) even though there is some contribution to the signal from depths up to ~0.3 μm, but with decreasing efficiency [19]. The Mössbauer measurements were made at room temperature using a ^{57}Co source in a rhodium matrix with an initial activity of 50 mCi. The specimen of interest was placed in gas flow proportional counter where 7.3 keV conversion electrons resulting from recoilless resonant absorption by ^{57}Fe nuclei within the specimen were detected. The velocity of the Mössbauer spectrometer was calibrated by recording a reference spectrum of a α-Fe phase present in metallic iron (Fig. 4a). The Mössbauer spectra recorded on each sample are presented in Fig. 4b–h. On each Mössbauer spectrum, we can observe the sextet due to α-Fe present in the low carbon steel substrate (same sextet as in Fig. 4a). When the deposition rate is decreasing, the relative area of the sextet increases. For all coatings, a doublet is observed with an isomer shift and a quadripole splitting of IS = 0.32 mm/s and QS = 0.6 mm/s, respectively. For the hydrogen flow upper than 4 sccm, a second doublet with an isomer shift of IS = 0.42 mm/s and a quadruple splitting of QS = 0.33 mm/s must be introduce to fit correctly the experimental spectra. The solid lines on each spectra of Fig. 4 reproduce the fits.

4. Results and discussion

As we can observe from Fig. 2a, the deposition rate decreases linearly when the hydrogen flow increases. This effect can be correlated with the partial pressure of Ar (Fig. 1), which is mainly responsible for the erosion of the sputter target. Regarding the evolution of the nitrogen partial pressure (Fig. 1) and the nitrogen concentration (Fig. 2b) vs. the hydrogen mass flow, we can also conclude that the nitriding of the coatings is

more efficient when hydrogen is mixed to the reactive gases. Depth profiles of nitrogen shown in Fig. 3a confirm those results. When hydrogen is only due to contamination of the reactive gases (coating number 1), the deposition rate is approximately 5×10^{15} at. cm^{-2} but the nitrogen concentration still under 30 at.% (solid line in Fig. 3a). The hydrogen depth profile (solid line in Fig. 3b) shows only a contamination at the surface, which is always present but also a peak at the interface. This local contribution has been attributed to hydrogen contamination of the substrate before deposition. As the hydrogen flow is increasing, the thickness of the depth profile of nitrogen (dashed line in Fig. 3a) is decreasing but the nitrogen concentration is higher than 30 at.%. The depth profiles of hydrogen (dashed line in Fig. 3b) show clearly a non-uniform distribution and an accumulation of hydrogen near the interface between the coating and the substrate. This effect has been observed for all measured depth profiles of hydrogen. It can be explained by the mobility of hydrogen, which is more important where the concentration of defects is important.

Combining PIXE and RBS analysis, we can observe that the relative iron, chromium and nickel compositions of all nitrogen-containing coatings are within the specifications of AISI 304L stainless steel. As the nitrogen content of the coating increased, these elements decreased proportionally indicating that iron, chromium and nickel atoms are transferred from the target to the sample in constant proportions. Shedden et al. [12] have also reported this behaviour. This is due to sputter yield amplification effect. The differences in partial sputtering yield for nickel, chromium and iron are very small (1.0, 1.1 and 1.0, respectively, for 500 eV Ar ions [20]) and result in target surface enrichment of the slowest sputtering element. The target quickly reaches a steady state condition, even though the target surface chemistry is altered.

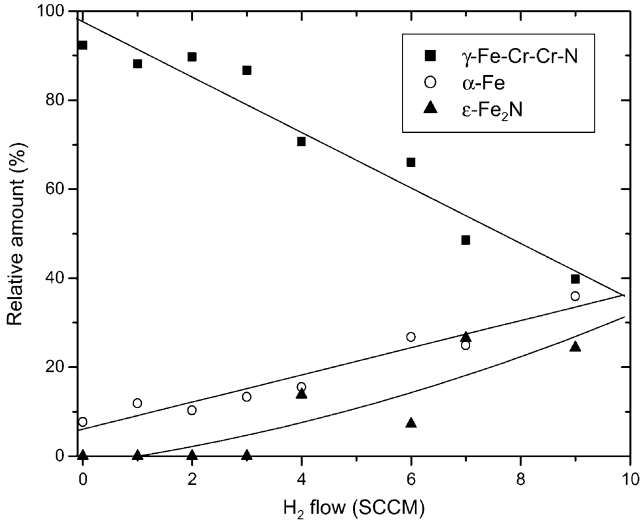

Fig. 5. Evolution of the relative amount of different phases observed using CEMS vs. the hydrogen mass flow.

Fig. 5 shows the relative amount of the different phases observed by CEMS. Using the data from Cook [21], the first doublet (IS = 0.32 mm/s, QS = 0.6 mm/s) has been attributed to γ_N-Fe-Cr-Cr-N, which is a typical Fe(III) sub spectrum [22], while the second doublet is due to ε–Fe_2N. It is clearly observed that the γ_N phase is decreasing when H_2 flow increases. This is

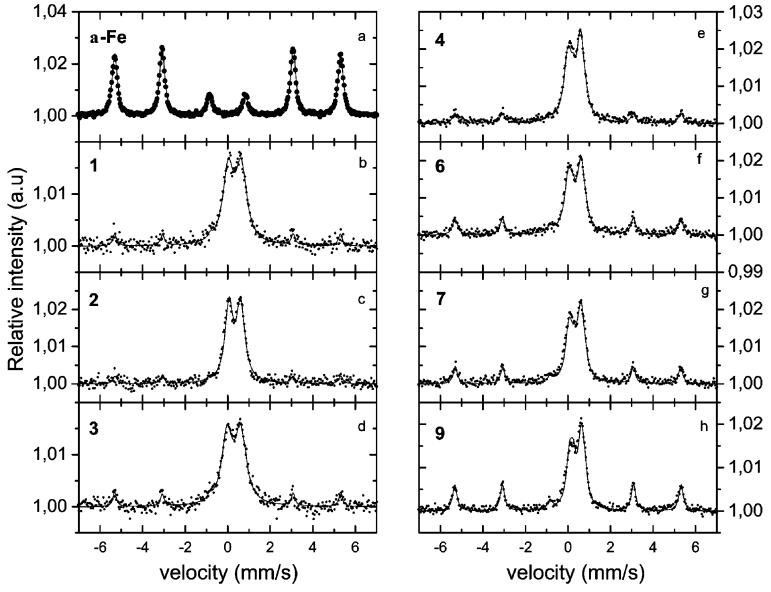

Fig. 4. Mössbauer spectra measured by CEMS on (a) α-Fe, (b–h) nitrided coatings deposited on low carbon steel substrates. The numbers indicated in the upper-left corner of each figure represent the hydrogen flows.

mainly due to the reducing thickness of the coatings because we can observe more and more α-Fe due to the substrate, but also to the ε-Fe_2N phase, which appears for H_2 flows higher than 4 sccm. For those flows, the maximum nitrogen concentration is 32 at. % and corresponds to the relative amount of nitrogen in the ε-Fe_2N phase.

5. Conclusions

Stainless steel coatings (AISI-304L cathode) deposited at room temperature by DC-magnetron sputtering in a reactive atmosphere containing N_2 and H_2 have been characterised quantitatively using different nuclear techniques. It has been shown that the deposition rate is directly related to the partial pressure of argon in the chamber. The nitriding of the coating is more efficient when hydrogen is mixed to the reactive gases and the nitrogen phase formed is richer. The nitrogen depth distribution in the layers is flat while hydrogen is mainly concentrated at the surface (contamination) and at the interface where the concentration of defects is more important. The relative amounts of iron, chromium and nickel in the coatings have been measured by PIXE and still in the same proportion than in the AISI 304L cathode target.

CEMS confirms the results observed by PIXE, RBS, NRA and RNRA. We have shown that at low flow of hydrogen, only Fe III is formed, while for higher hydrogen flows, the stoichiometric ε-Fe_2N phase appears.

References

[1] G. Wagner, T. Louis, R. Leutenecker, U. Gonser, Hyperfine Interactions 46 (1989) 501.
[2] T.h. Briglia, G. Terwagne, F. Bodart, C. Qwaeyhaegens, J. D'Haen, L.M. Stals, Surf. Coat. Technol. 80 (1996) 105.
[3] D.L. Williamson, J.A. Davies, P.J. Wilbur, Surf. Coat. Technol. 103–104 (1998) 178.
[4] O. Oztürk, D.L. Williamson, J. Appl. Phys. 77 (1995) 3839.
[5] E. Menthe, K.-T. Rie, J.W. Schultze, S. Simson, Surf. Coat. Technol. 74–75 (1995) 412.
[6] G.A. Collins, R. Hutchings, J. Tendys, Mater. Sci. Eng. A139 (1991) 171.
[7] K. Ichii, K. Fujimura, T. Takase, Technol. Rep. Kansai Univ. 27 (1986) 135.
[8] M.P. Fewell, D.R.G. Michell, J.M. Priest, K.T. Short, G.A. Collins, Surf. Coat. Technol. 131 (2000) 300.
[9] S.D. Dahlgren, Metall. Trans. 1 (1970) 3095.
[10] A. Bourjot, M. Foos, C. Frantz, Surf. Coat. Technol. 43–44 (1990) 533.
[11] K.L. Dahm, P.A. Dearnley, Surf. Eng. 12 (1996) 61.
[12] B.A. Shedden, F.N. Kaul, M. Samandi, B. Window, Surf. Coat. Technol. 97 (1997) 102.
[13] G. Terwagne, J. Colaux, G.A. Collins, F. Bodart, Thin Solid Films 377–378 (2000) 441.
[14] S. Kumar, M.J. Baldwin, M.P. Fewell, S.C. Haydon, K.T. Short, G.A. Collins, et al., Surf. Coat. Technol. 123 (2000) 29.
[15] G. Terwagne, to be published.
[16] G. Terwagne, M. Piette, F. Bodart, Nucl. Instr. Meth. B19/20 (1987) 145.
[17] B. Maurel, G. Amsel, Nucl. Instr. Meth. 218 (1983) 159.
[18] W.A. Landford, Nucl. Instr. Meth. B66 (1992) 65.
[19] D.L. Williamson, F.M. Kustas, M.S. Misra, J. Appl. Phys. 60 (1986) 1493.
[20] D.M. Hoffman, B. Singh, J.H. Thomas III, Handbook of Vacuum Science and Technology San Diego: Academic Press, (1998) 611.
[21] D.C. Cook, Met. Trans. A18 (1987) 201.
[22] T. Kacsich, M. Niederdrenk, P. Schaaf, K.P. Lieb, U. Geyer, O. Schulte, Surf. Coat. Technol. 93 (1997) 32.